Dissociation of $^{13}CH_4$ and $^{15}N_2$ and the global transport of impurities in an ASDEX Upgrade L-mode plasma

J. Miettunen[1], M.I. Airila[2], T. Makkonen[1], M. Groth[1], V. Lindholm[1], C. Björkas[3], A. Hakola[2], H.W. Müller[4] and the ASDEX Upgrade Team[4]

[1] *Department of Applied Physics, Aalto University, P.O. Box 14100, 00076 AALTO, Finland*

[2] *VTT Technical Research Centre of Finland, P.O. Box 1000, 02044 VTT, Finland*

[3] *Department of Physics, University of Helsinki, P.O. Box 43, FI-00014 Helsinki, Finland*

[4] *Max-Planck-Institut für Plasmaphysik, 85748 Garching, Germany*

Introduction

Trace-element injection experiments are one of the few controlled methods for studying global impurity migration in tokamaks. In these experiments, a trace element is injected into the plasma in a molecular form, such as $^{13}CH_4$ and its subsequent deposition around the torus can be studied with post mortem analysis of samples from selected wall tiles [1].

In this contribution, we use the 3D impurity transport code ERO to study the dissociation of injected $^{13}CH_4$ and $^{15}N_2$ molecules in L-mode plasma conditions resembling a high-density experiment on ASDEX Upgrade (AUG) in 2011. The global transport and deposition of the born ^{13}C and ^{15}N ions is then modelled using the 3D orbit-following code ASCOT. In particular, we address the impact of increasing plasma density on the dissociation and the transport of the ions.

Modelling of $^{13}CH_4$ and $^{15}N_2$ dissociation using the ERO code

In general, the reaction chain starting from an injected molecule entering the plasma and ending in the generation of one or several singly charged trace ions is highly complex. For example, methane in the form of $^{13}CH_4$ can first be ionized to $^{13}CH_4^+$ or dissociated into neutral or ionized $^{13}CH_3$ [2]. In the following steps, the molecules can again be either ionized or dissociated into smaller fragments until reaching a point where a single $^{13}C^+$ ion is born.

In 2011, the injection was performed from a port at the outer (low-field side) midplane in the toroidal sector 9 of AUG. For modelling $^{13}CH_4$ and $^{15}N_2$ dissociation with ERO, the simulation setup included a magnetic equilibrium for the discharge #27385 at 4.0 s, a 2D geometry of the injection port in an (*R,z*) plane and the molecules were injected 1.24 m away radially from the closest wall tiles following a Maxwellian distribution with a mean initial energy of 0.05 eV.

Several background plasma solutions in the scrape-off layer (SOL) near the separatrix were generated using the SOLPS code package. At an input power of 2 MW, a density scan was performed by raising the outer midplane separatrix electron density from $n_{e,sep,OMP} = 1.0 \cdot 10^{19}$ 1/m^3

to $2.25 \cdot 10^{19}$ 1/m^3 and then to $3.0 \cdot 10^{19}$ 1/m^3. For the electron temperature, $T_{e,OMP}$, a reasonable match with experimentally measured profiles was found, but the electron density profiles, $n_{e,OMP}$, were observed to have a much stronger radial decay compared to the experimental measurements. Increasing the density at the OMP separatrix was seen to mainly decrease T_e in the core plasma while maintaining the SOL plasma at an approximately constant temperature. As the flow velocity calculated with SOLPS was unrealistically low (mostly below Mach 0.2), a manually imposed plasma flow of Mach 0.5 in the main chamber region was used for the ERO and ASCOT simulations.

Radially outside the SOLPS calculation grid in the far-SOL and halo plasma, the plasma temperature and density values were extrapolated as exponentially decaying with decay lengths $\lambda_{T_e} = \lambda_{T_i} = 5.0$ cm and $\lambda_{n_e} = \lambda_{n_i} = 2.2$ cm obtained from fits to AUG midplane manipulator measurements during a reference discharge #27371 for the experiment. Inside the injection port, the connection length is greatly shortened which then results in a faster decay of the profiles. In this region, a value of $\lambda = 0.5$ cm was used for both density and temperature based on previous measurements on AUG with a ball-pen probe [3].

With ERO, the molecules were followed until an ion ($^{13}C^+$ or $^{15}N^+$) was born. For modelling the dissociation of $^{15}N_2$, the required cross section data was added into the code [1].

Ionization profiles of Fig. 1 obtained from these simulations show that the dissociation is not strongly localized around any specific location but, instead, the radial profiles are wide extending into the far-SOL. With increasing density, the dissociation is noticeably shifted towards the wall (injection location) and thus only a very small number of the ions are born near the separatrix at R_{sep}. Although not shown here, the profiles for the mid-density case were observed to lie between the shown cases of low and high density. In the z direction of the (R,z) plane the ions formed a rather uniform cloud with the approximate size of the outer wall limiter next to the injection port.

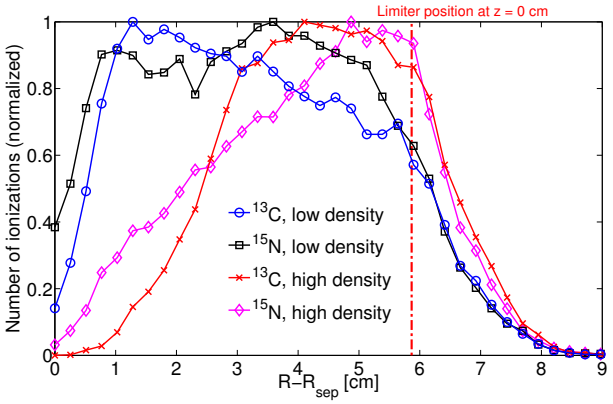

Figure 1: *Radial ionization profiles in the low and high density cases.*

When comparing the locations of the highest dissociation peaks in Fig. 1, it is observed that the peaks for nitrogen are closer to the wall than for carbon. However, more ^{15}N ions are born also in the vicinity of the separatrix. The overall effect is that the average radial position of the born ions, $\overline{R - R_{sep}}$, is slightly closer to the wall for ^{13}C. As a function of density, the average

values were approximately $\overline{R-R_{sep}} = 3.5$–$4.6$ cm for carbon and $\overline{R-R_{sep}} = 3.4$–$4.4$ cm for nitrogen. Thus, only minor differences between the two species were observed.

Global transport and deposition of ^{13}C and ^{15}N ions

The resulting ionization clouds from the ERO simulations were used as an input for ASCOT by taking the (*R*,*z*) locations of the ions, their initial energies and directions of velocity and giving them a random toroidal angle $\phi = 182 - 201^\circ$ (the toroidal extent of the injection port) as the ERO modelling does not result in a toroidal ionization distribution. All of the test particles were then followed with ASCOT until their deposition on the wall.

In the ASCOT simulations, a 3D wall geometry of AUG based on CAD data was used obtain detailed deposition patterns of the followed particles. The magnetic field and the background plasma outside the separatrix were the same as in the ERO simulations except for the addition of toroidal ripple for the ASCOT magnetic field. In the core plasma, 1D profiles of temperature and density were used based on data from various diagnostics of the discharge #27385. The coefficient for anomalous radial diffusion was set to a constant value of $D_\perp = 0.25$ m^2/s.

Figure 2 shows that with increasing density, the deposition of ^{13}C and ^{15}N is shifted away from the divertor region towards the main chamber. Clearly, deposition at both the inner and outer divertor decreases whereas increased deposition is seen at the inner and outer wall and the top of the vessel. The difference between carbon and nitrogen is small with slightly more carbon being deposited in the main chamber. This is in agreement with the observation from ERO that the average ionization location was by a minor difference closer to the wall for $^{13}CH_4$ than for $^{15}N_2$.

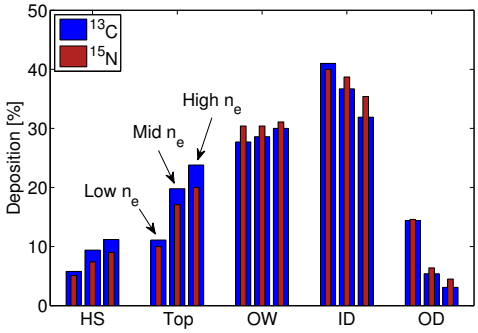

Figure 2: *Deposition in large-scale regions with increasing n_e. Here, HS stands for the inner wall heat shield, Top for the top of the vessel, OW for the outer wall with ID and OD denoting the inner and outer divertors.*

At least two major mechanisms can be found to contribute to the effect of increasing density on the large-scale deposition. First, as shown previously, the injected molecules dissociate closer to the wall as density is increased. When considering the topology of magnetic flux surfaces in the SOL, it is notable that close to the separatrix the flux surfaces connect the inner and outer divertors. Radially outwards and thus closer to the wall, however, the flux surfaces are fully outside the divertor region and connect, e.g., the outer wall and the top of the vessel. Consequently, dissociation closer to the wall increases the probability for main chamber deposition.

In addition to this mechanism originating in molecule dissociation, increasing density also

affects the global transport of the born ions. Importantly, the collision frequency of the impurity ions with the background plasma is proportional to the background plasma density. Thus, with increasing density the ions become more strongly coupled with the background plasma and, crucially, the plasma flow. Near the injection location, the flow is directed towards the inner divertor through the top of the plasma. The effect of stronger coupling between the ions and the background plasma is therefore seen as an increase in transport towards these regions.

The 2D deposition distribution shown in Fig. 3 exhibits similar features as reported in [4]. At the outer wall, the deposition pattern is strongly toroidally asymmetric whereas other parts of the vessel indicate rather symmetric deposition. A similar distribution was observed also for ^{15}N and the increase in plasma density was seen to mainly concentrate the deposition more strongly around the injection location.

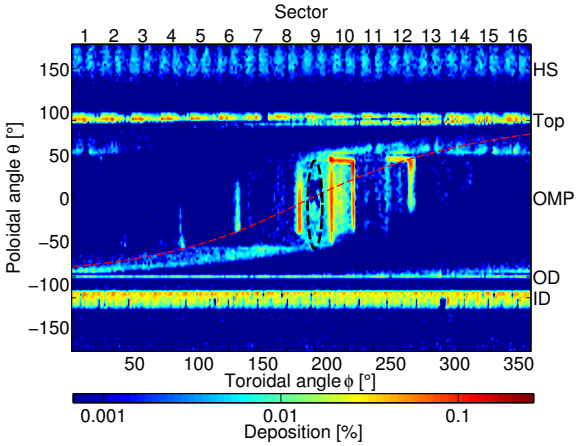

Figure 3: *2D deposition distribution of ^{13}C in the mid-density case showing also the injection port (ellipse) and the magnetic field line structure at the low-field side (dashed).*

Conclusions

The presented modelling suggests that the dissociation of injected $^{13}CH_4$ and $^{15}N_2$ molecules can occur relatively far from the separatrix and moves closer to the wall with increasing plasma density. Owing to this and the increasing collisionality with density, the global deposition of ^{13}C and ^{15}N was observed to be shifted from the divertor towards the main chamber. Comparing carbon and nitrogen, only minor differences were observed in the dissociation of the molecules and the resulting deposition pattern. However, the analysis presented here neglects plasma-surface interaction effects which, experimentally, have been observed to cause even qualitatively different deposition patterns for the two species [1]. In addition, the described effect of increasing density considers only the primary deposition location not taking into account further erosion of deposited particles.

Acknowledgements

This work, supported by the European Communities under the contract of Association between Euratom/Tekes, was carried out within the framework of the ITER Physics Support Activities of the European Fusion Development Agreement. The views and opinions expressed herein do not necessarily reflect those of the European Commission. This work was partially funded by the Academy of Finland project No. 259675.

References

[1] A. Hakola et al., this conference, I1.001
[2] R.K. Janev and D. Reiter, Phys. Plasmas **9**, 4071 (2002)
[3] J. Horacek et al., Nucl. Fusion **50**, 105001 (2010)
[4] J. Miettunen et al., Nucl. Fusion **52**, 032001 (2012)